Localization of notches with Lamb waves

Rüdiger Benz
School of Civil and Environmental Engineering, Georgia Institute of Technology, Atlanta, Georgia 30332-0355

Marc Niethammer
School of Electrical and Computer Engineering, Georgia Institute of Technology, Atlanta, Georgia 30332-0250

Stefan Hurlebaus
Institute A of Mechanics, University of Stuttgart, Allmandring 5 b, D-70550 Stuttgart, Germany

Laurence J. Jacobs[a)]
School of Civil and Environmental Engineering and G. W. Woodruff School of Mechanical Engineering, Georgia Institute of Technology, Atlanta, Georgia 30332-0355

(Received 5 February 2003; revised 20 May 2003; accepted 30 May 2003)

A time–frequency representation (TFR) is used to analyze the interaction of a multimode and dispersive Lamb wave with a notch, and then serves as the basis for a correlation technique to locate the notch. The experimental procedure uses a laser source and a dual-probe laser interferometer to generate and detect Lamb waves in a notched plate. The high fidelity, broad-bandwidth, point-like and noncontact nature of laser ultrasonics are critical to the success of this study, making it possible to experimentally measure transient Lamb waves without any frequency biases. A specific TFR, the reassigned spectrogram, is used to resolve the dispersion curves of the individual modes of the plate, and then the slowness-frequency representation (SFR) of the plate is calculated from this reassigned spectrogram. By considering the notch to be an additional (second) source, the reflected and transmitted contributions of each Lamb mode are automatically identified using the SFRs. These results are then used to develop a quantitative understanding of the interaction of an incident Lamb wave with a notch, helping to identify mode conversion. Finally, two complementary, automated localization techniques are developed based on this understanding of scattering of Lamb waves.
 [DOI: 10.1121/1.1593058]

PACS numbers: 43.20.Mv, 43.35.Cg [YHB]

I. INTRODUCTION

Our objective in this research is to develop an automated methodology that uses multimode and dispersive Lamb waves to locate a notch. The experimental procedure uses a laser source and a dual-probe laser interferometer to generate and detect Lamb waves in both notched and perfect plates. The high fidelity, broad-bandwidth, point-like, and noncontact nature of laser ultrasonics are critical to the success of this study, making it possible to measure transient Lamb waves without any frequency biases. Experimentally measured time–domain Lamb waves are first transformed into the time–frequency domain by calculating the reassigned spectrogram, a time–frequency representation (TFR); this TFR resolves the individual modes of the plate and generates its dispersion curves. The reassigned spectrogram is then normalized with respect to propagation distance by converting it to a slowness-frequency representation (SFR)—this is a quick and simple calculation.

A procedure is then developed to identify the reflected and transmitted contributions of each Lamb mode by considering the notch to be an additional (second) source. The SFRs from each of the interferometric probes (and in both the perfect and notched plates) are compared, and modes are automatically classified into different cases, depending on their interaction with the notch. These results are used to develop a quantitative understanding of the interaction of an incident Lamb wave with a notch, helping to identify mode conversion.

Finally, two complementary, automated localization techniques are developed based on this understanding of the scattering of Lamb waves. One technique isolates the contributions of the signal reflected from the notch by performing a correlation of a series of SFR spectra, each calculated with different, assumed propagation distances. This correlation technique uses an understanding of Lamb wave scattering—for example, the knowledge such as which modes are reflected, but not mode converted (and through which frequencies) helps refine the proposed correlation localization procedure. The second technique uses a goodness-of-fit metric when allocating (identifying) the transmitted, and mode converted wave field to determine the notch location. These two complementary techniques can be combined to provide two independent predictions (and thus increase accuracy), or can be used separately. Considering the arbitrary nature of the geometric relationship between the notch, the source, and each of the receivers in a real application, this robustness is especially important; the effectiveness of the proposed local-

[a)]Author to whom correspondence should be addressed. Electronic mail: laurence.jacobs@ce.gatech.edu

ization procedure is not dependent on the notch being located between the laser source and the receivers.

Previous researchers have used Lamb waves for material characterization (see Chimenti[1] for details), but a Lamb wave's multimode and dispersive nature makes an interpretation of time–domain signals difficult. In contrast, TFRs operate on time–domain signals, are capable of resolving the individual modes of a plate, and naturally lead to the slowness-frequency representation. TFRs are well known in the signal processing community (see Cohen[2] for a review of TFRs). Previous research has shown that TFRs based on the short-time Fourier transform (STFT)—spectrogram, reassigned spectrogram[3]—and the (pseudo) Wigner–Ville distribution[4] are particularly well suited for representing Lamb waves. The spectrogram is effective in this application because of its constant time–frequency resolution over all times and frequencies.[3] Lemistre *et al.*[5] and Wilcox *et al.*[6] used the TFRs of Lamb waves for the damage detection in composite plates, while Valle *et al.*[7] used time-of-flight information calculated from a reassigned spectrogram to locate notches in cylinders. Hurlebaus *et al.*[8] used the TFRs of Lamb waves and a correlation of the reflected contribution to localize notches in plates, but their research does not require (nor was it developed with) an understanding of the scattering of a Lamb wave by a notch.

Previous researchers have studied the interaction of guided Lamb waves with a crack. Liu *et al.*[9] investigated transient scattering of Lamb waves by a surface-breaking crack, while Cho and Rose[10] applied the boundary element method to determine the transmission and reflection coefficients from a surface breaking defect. Lowe and Diligent,[11] and Diligent *et al.*[12] examined the scattering of the lowest symmetric (s_0) mode from both a rectangular notch, and from a through thickness hole, respectively. Castaings *et al.*[13] used modal decomposition and an air-coupled ultrasonic receiver to model the interaction of Lamb waves with a crack; this study used the noncontact and high fidelity nature of air-coupled ultrasound, and generated selected modes (through a limited frequency bandwidth) with an interdigital-like (IDT) transmitter. This is in contrast to the current research that generates a broadband, multimode Lamb wave, and then relies on signal processing (the reassigned spectrogram) to resolve the individual modes of the plate. Note that an alternative approach is to use the two-dimensional Fourier transform (2D-FT)[14,15] to develop the dispersion curves. The 2D-FT is robust, but has the disadvantage that it requires multiple, equally spaced waveforms. In contrast, the current approach only requires a single waveform, while the processing involved in transforming this single time–domain Lamb wave to a SFR is computationally straightforward, and can be easily automated.

II. EXPERIMENTAL PROCEDURE, TIME–FREQUENCY AND SLOWNESS-FREQUENCY REPRESENTATIONS

The experimental procedure makes high fidelity, resonance-free, point-like noncontact measurements of Lamb waves over a wide frequency range (100 kHz to 10 MHz). Broadband Lamb waves are generated with an Nd:YAG laser source (see Scruby and Drain[16] for details on laser ultrasonics). Laser detection of these waves is accomplished with a dual-probe, heterodyne laser interferometer originally developed by Bruttomesso *et al.*,[17] and extended by Hurlebaus[18] to be a dual-probe receiver. This instrument uses the Doppler shift to simultaneously measure out-of-plane surface velocity (particle velocity) at two points on the surface of the plate. The Nd:YAG laser fires (at $t=0$) and generates a Lamb wave at the source location (ablation source). This Lamb wave is independently measured by each of the interferometric probes (as a transient, time–domain signal), discretized using a digital oscilloscope with a sampling frequency of 100 MHz, low-passed filtered (a linear phase analog Bessel filter) at 10 MHz, and averaged over 60 Nd:YAG shots (to increase the signal-to-noise ratio).

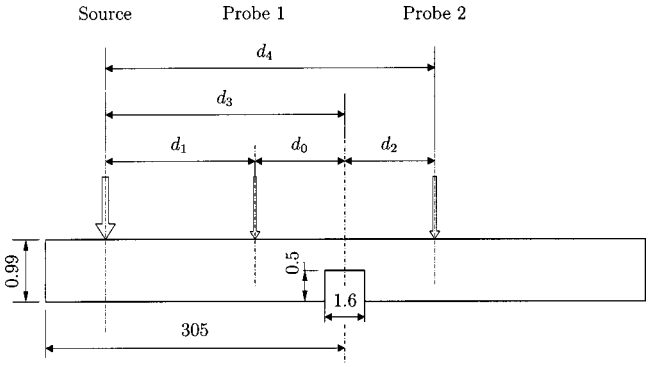

FIG. 1. Experimental setup (dimensions in mm).

Two different plate specimens are considered in this research. One plate specimen has no defects and is identified as the ''perfect plate,'' while the second has a single milled notch and is referred to as the ''notched plate''—the plates are identical otherwise, made of 3003 aluminum, with dimensions of 305 mm$\times$610 mm$\times$0.99 mm. The notch has a depth of 0.5 ± 0.1 mm, a width, w, of 1.6 ± 0.1 mm, a length of 305 mm (full plate width) and is located on the centerline of the 610 mm dimension of the plate. The relatively large plate size (305 mm$\times$610 mm) is needed to minimize the interference of reflections from the plate edges and all measurements are made in the center of the plate. Figure 1 shows the notched plate specimen, together with the location of the laser source and each of the two interferometric probes—the source and probe 1 are always on one side of the notch, while probe 2 is on the opposite side of the notch. Note that the source and both receiving probes are on the same face of the plate, while the notch is on the opposite (inaccessible) face. d_1 is the distance from source to probe 1, d_0 is the distance from probe 1 to the centerline of the notch, and d_2 is the distance from the centerline of the notch to probe 2. Define $d_3=d_1+d_0$, $d_4=d_3+d_2$, and $d_5=d_1+2d_0$. Lamb waves are measured at a variety of propagation distances (for comparison and verification purposes) by holding d_0 and d_2 fixed (30 mm each, which is approximately 30 plate thicknesses) for all experiments, and varying d_1 from 50 to 85 mm (in 5 mm increments).

A time–domain Lamb wave signal is transformed into the time–frequency domain using the STFT, essentially chopping the signal into a series of small overlapping pieces. Each of these pieces is windowed and then individually Fou-

rier transformed.[2] The STFT of a time–domain signal, $s(t)$, is defined as

$$S(\omega,t)=\frac{1}{2\pi}\int_{-\infty}^{\infty} e^{-i\omega\tau}s(\tau)h(\tau-t)\mathrm{d}\tau, \tag{1}$$

where $h(t)$ is the window function and ω is angular frequency. The energy density spectrum of a STFT is defined as

$$E_d(\omega,t)=|S(\omega,t)|^2, \tag{2}$$

and is called a spectrogram.

TFRs such as the spectrogram suffer from the Heisenberg uncertainty principle, making it impossible to simultaneously have perfect resolution in both time and frequency.[2] The resolutions in time and frequency are related to each other, and limited by the inequality, $\sigma_t^2\sigma_w^2\geqslant 0.25$, where σ_t and σ_w are the standard deviations for time and frequency, respectively. The equality holds for a Gaussian window [$h(t)$ in Eq. (1)]; the current research uses a Hanning window to compute the STFT because it allows for relatively small signal distortion, while ensuring smoothness of the windowed signal.[19] The time–frequency resolution of a spectrogram is solely controlled by the window size and type, and is independent of frequency. Choosing a narrow window provides for good resolution in time, but poor resolution in frequency, whereas a wide window leads to better frequency resolution and worse time resolution. This study uses a 384-point window for the time–domain signals measured at a 100 MHz sampling frequency (see Niethammer *et al.*[3] for details).

An improvement in the time–frequency resolution of a spectrogram is achieved by applying the reassignment method, developed by Auger and Flandrin.[20] The reassignment method reduces the time–frequency spread of a spectrogram by relocating ''energy'' from its old position, coordinates (t, ω), to new, reassigned coordinates, $(\hat{t},\hat{\omega})$.

The reassigned spectrogram transforms an experimentally measured time–domain Lamb wave signal into the time–frequency domain. This transformation enables a more quantitative interpretation of the Lamb wave,[3] but it is still difficult to compare reassigned spectrograms of measurements made with different propagation distances. This difficulty is due to the fact that arrival time is a function of propagation distance, which causes different time shifts for different propagation distances. It is possible to normalize these Lamb waves with respect to propagation distance by considering either the group velocity–frequency representation, or the slowness-frequency representation (SFR). Define group velocity, c_g, for any propagation distance, d, and time, t (for each frequency) as $c_g=d/t$, while (energy) slowness, sl_e, is defined as $sl_e=t/d$.

The calculation of group velocity from a TFR (like the reassigned spectrogram) with a fixed propagation distance d is a nonlinear operation in t that transforms an equally spaced time grid to an unequally spaced grid in group velocity, c_g. This is in contrast to the slowness transformation, which is a linear operation in t—the equally spaced time grid is transformed to an equally spaced grid in (energy) slowness, sl_e. Transformation nonlinearities are avoided by selecting the SFR to represent the experimentally measured time–domain Lamb wave signals.

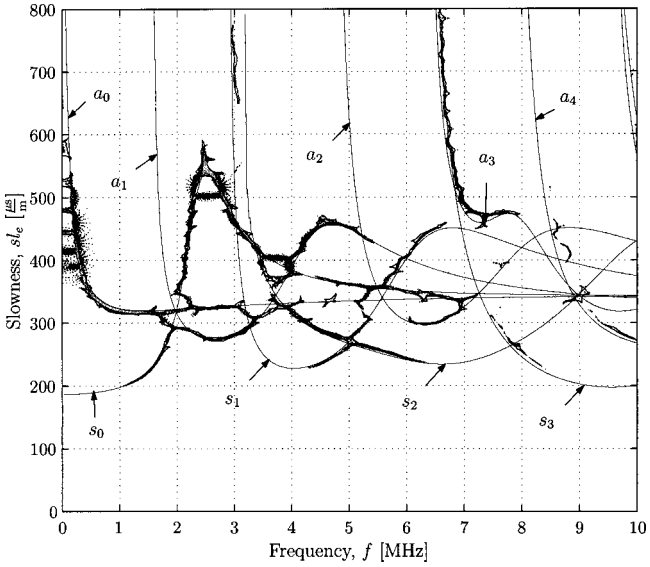

FIG. 2. SFR of perfect plate.

III. EXPERIMENTAL INTERACTION OF A LAMB WAVE WITH A NOTCH

Figure 2 shows the square root (for better visibility) of the energy density spectrum of the SFR (obtained from the reassigned spectrogram) measured in the perfect plate for a propagation distance of 70 mm, together with the theoretical Rayleigh–Lamb solution,[21] presented as solid lines and identified as either symmetric, s_i, or antisymmetric, a_i, modes. There is excellent definition of seven experimentally measured modes (s_0-s_2 and a_0-a_3) and all these experimental modes match the theoretical solution (no experimental modes are unaccounted for). Interference during the reassignment procedure causes some ''fuzziness'' in the vicinity of the intersection of modes.[3] Note that Fig. 2 is also a representation of the propensity of a particular mode to be excited by the laser source (and noting that the laser interferometer used in this study only measures out-of-plane motion), meaning that not all portions of a mode (e.g., a_1 below 2 MHz) can be considered in this study. However, Fig. 2 can be thought of as the SFR of the Lamb wave that is incident on the notch (in the notched plate specimen).

Now consider SFRs for the notched plate. Note that the notch location is now assumed to be *known* in order to study the scattering phenomena; this knowledge will then be used to determine an unknown notch location in Sec. IV. Figures 3(a)–(b) show the SFRs for propagation distances of 70 mm (d_1) and 130 mm (d_4)—simultaneously measured by probes 1 and 2, respectively—together with the theoretical solution for the *perfect plate*, presented as solid lines. Modes above a slowness of about 650 μs/m in Fig. 3(b) that do not match any theoretical mode lines are due to reflections from the plate edges, are spurious, and are not included in the following discussions. A comparison of SFRs of the perfect plate and the notched plate shows that a significant portion of the

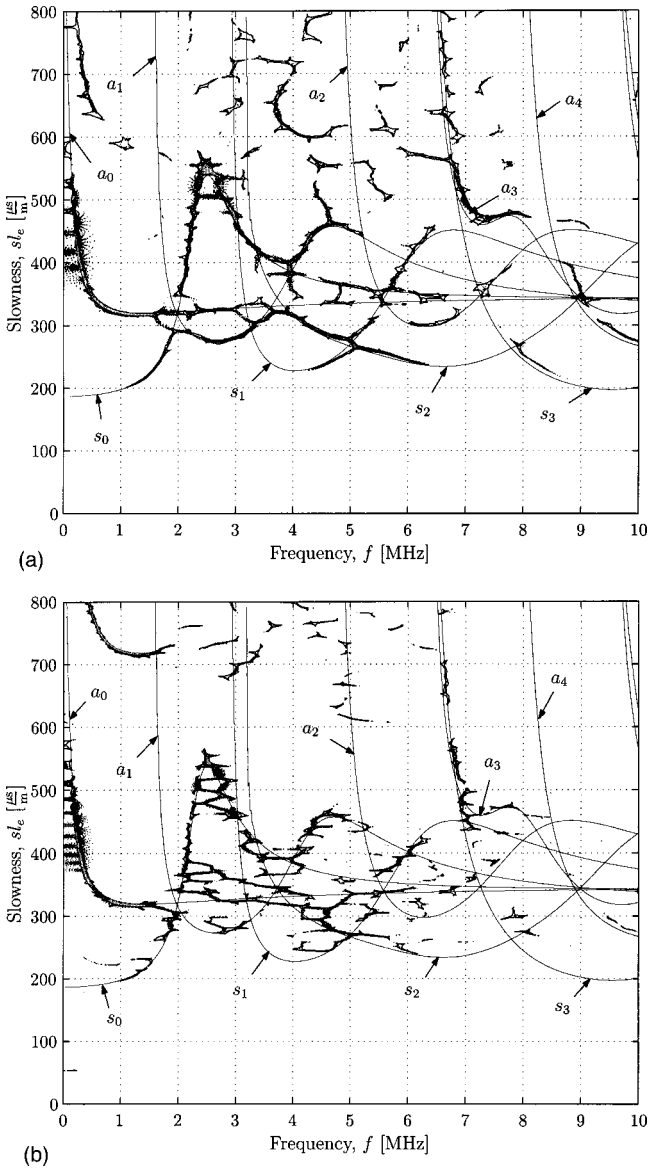

FIG. 3. (a). SFR of notched plate, Probe 1, source to receiver distance (d_1) of 70 mm. (b) SFR of notched plate, Probe 2, source to receiver distance (d_4) of 130 mm.

energy in the notched plate still corresponds to the theoretical solution of the perfect plate. However, the notched plate SFRs show additional modes that are not present in the perfect plate SFR, and these additional modes do not fit any theoretical mode lines.

First, compare the probe 1 signal of the notched plate [Fig. 3(a)] with the perfect plate (Fig. 2). The SFR of the notched plate has additional modes for slownesses larger than 500 μs/m that are the contribution of the Lamb wave that is reflected from the notch. The perfect plate SFR contains only the incident signal, while the probe 1 notched plate SFR contains both the incident and reflected (from the notch) signals. The reflected signal occurs at a later time (higher slowness) because it has a longer propagation distance. If the probe 1 TFR was transformed with a propagation distance, d, that corresponds to the source to notch to receiver distance, d_5, instead of the source to receiver distance [d_1 of 70 mm used to calculate the SFR in Fig. 3(a)], the resulting SFR would highlight the reflected modes.[19] The reflected (and nonconverted) modes in this SFR would coincide with the theoretical modes. This ''reflected'' SFR would also contain modes that do not fit the theoretical solution—referred to as *extraneous modes*—which will be discussed in detail later.

Now, compare the probe 2 signal for the notched plate [Fig. 3(b)] with the perfect plate (Fig. 2). The probe 2 SFR only contains the transmitted portion of the signal, and Fig. 3(b) shows modes that do not fit the theoretical solution. These modes (e.g., between 300–500 μs/m, 2–4 MHz) are also identified as extraneous modes, and are due to the interaction of the incident Lamb wave with the notch.

An explanation of extraneous modes is based on a hypothesis that treats the notch as an additional (second) source that ''creates'' the reflected and transmitted modes. In addition, this development recognizes that these reflected and transmitted modes all propagate within the same plate, so they should all be able to be represented as the theoretical modes of the perfect plate—all modes must satisfy the Rayleigh–Lamb equations of the perfect plate. These extraneous modes violate this requirement (they do not fall on a theoretical mode line) because the SFRs are calculated under the (possibly incorrect) assumption that the same mode propagates from the laser source to the notch, and then from the notch to the receiver (either probe 1 or probe 2). If this were truly the case, then there would be no extraneous modes present.

The scattering of Lamb waves by a notch is a complicated process, with mode conversion, and a number of other phenomena possible. Mode conversion in this context means that the energy propagates with mode i during the propagation from the laser source to the notch, and with a different mode, j, during the propagation from notch to receiver. Internal reflections (within the notch),[11] nonpropagating modes,[13] and local frequency (or phase) shifts are additional phenomena that can also be part of this scattering process. Instead of approaching this problem from an energy conservation approach, this research develops a systematic procedure to identify which modes (and through which frequencies) are transmitted and reflected, with or without mode conversion. Note that the proposed procedure does not consider internal reflections or local frequency shifts, but the success of the proposed localization technique (presented in Sec. IV) shows that these contributions are probably relatively small.

Consider a nomenclature where signals measured in the notched plate with probe 1 are classified as case P1a, incident; case P1b, reflected and non-mode-converted; and case P1c, reflected and mode converted. Signals measured in the notched plate with probe 2 are classified as case P2b, transmitted and non-mode-converted; and case P2c, transmitted and mode converted.

Since both the incident and the reflected signals are present in probe 1 measurements, case P1 is inherently more complicated, so examine case P2 (transmitted only) first. Consider a procedure that is used to accentuate the modes that coincide with the theoretical solution. This procedure entails multiplying a SFR with a *theoretical mode matrix*, $T(sl_e, f)$—this theoretical mode matrix is a three-

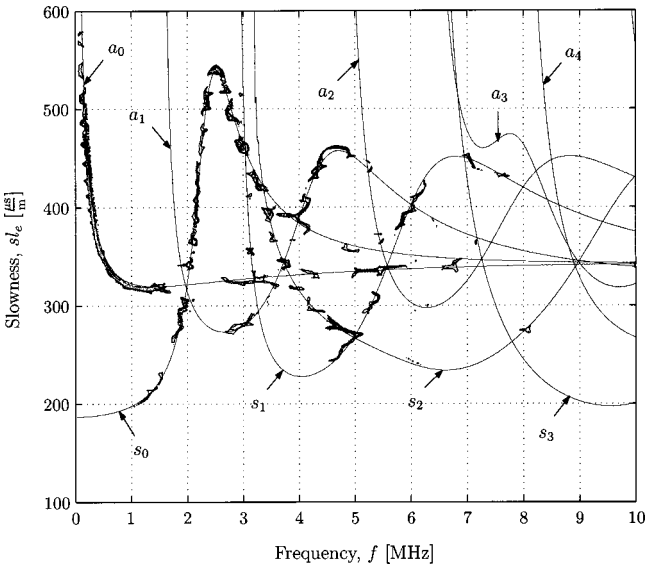

FIG. 4. SFR of modes belonging to case P2b, transmitted and non-mode-converted.

dimensional representation of the Rayleigh–Lamb equations that accounts for possible measurement uncertainties. $T(sl_e, f)$ equals unity on the set of slowness-frequency pairs that correspond to the solution of the Rayleigh–Lamb equations, and is smoothed out by Gaussian filtering in the slowness and frequency directions. Each mode is filtered individually, the respective maxima (the ridge values) are set equal to unity, and the individual modes are combined by taking the maximum over all modes (this guarantees a value of unity at mode intersections). The *inverse theoretical mode matrix*—a value of zero at the theoretical mode values (Gaussian curve), unity everywhere else—is obtained by subtracting the theoretical mode matrix from a matrix completely populated with ones.

Modes that belong to case P2b are comparatively easy to identify; modes that lie close to the theoretical mode lines in the SFR of the probe 2 signal, calculated with propagation distance d_4, are not mode converted at the notch. Thus, the SFR of Fig. 3(b) is multiplied by the theoretical mode matrix, and Fig. 4 shows the result—modes that are transmitted and not mode converted.

Modes not assigned to case P2b are considered to be extraneous and portions of these modes are systematically identified as belonging to case P2c. First, remove case P2b modes from the signal measured by probe 2 by multiplying the SFR in Fig. 3(b) with the inverse theoretical mode matrix. Define the propagation time from source to probe 2 as time t_4, and express this time as the sum of the time from source to notch, t_3, plus the time from notch to probe 2, t_2, or $t_4 = t_3 + t_2$. The slowness associated with the propagation over distance d_3, from source to notch, is defined as $sl_{e3} = t_3/d_3$, and the slowness associated with the propagation from notch to probe 2 is $sl_{e2} = t_2/d_2$. Finally, the slowness from source to probe 2 is $sl_{e4} = t_4/d_4$—this is the slowness shown in the SFR of Fig. 3(b). These slownesses are combined, and, after some simple algebra,

$$sl_{e3} = \frac{d_4 sl_{e4} - (d_4 - d_3) sl_{e2}}{d_3}. \tag{3}$$

Equation (3) relates the *unknown* slowness from source to notch (sl_{e3}), to the *known* slowness from source to receiver (sl_{e4}), and an *assumed* slowness from notch to receiver (sl_{e2}). The unknown slowness sl_{e3} can be calculated for every possible slowness-frequency combination through the relevant slowness range and frequency bandwidth. Consider only six modes—a_0, a_1, a_2, s_0, s_1, and s_2—these modes carry most of the experimentally measured energy. Six new SFRs are calculated (one for each of these six modes), each assuming all of the energy propagates from the notch to probe 2 with that particular mode. The slowness-frequency values for these modes are obtained from the theoretical solution[21] and go into Eq. (3) as the assumed sl_{e2}. All distances and sl_{e4} are *known* and thus the slowness sl_{e3} can be calculated for each frequency.

An algorithm that follows this procedure is programmed into MATLAB to develop an automated and objective way to (possibly) allocate the extraneous modes into one of these six possible transmitted modes. First, separate the modes that belong to case P2c, and then pick any point on the P2c SFR and do the following.

(1) Compute sl_{e3} for this point for each of the six possible modes: $a_0 - a_2$ and $s_0 - s_2$.

(2) Next, compare the magnitude of the theoretical mode matrix, $T(sl_{e3}, f)$, at each of the six slowness-frequency pairs calculated in step 1. Select the slowness-frequency pair that has the largest magnitude. This defines the mode type propagating from laser source to notch. This is a modified probabilistic approach that searches for the mode that is most likely to be the match, since $T(sl_{e3}, f)$ is similar to a two-dimensional probability distribution function, although not in the strict mathematical sense.

(3) The entire propagation path is now defined—from laser source to notch with the slowness corresponding to the mode selected in step (2), and then from the notch to the receiver (probe 2), by looking at the mode that it is mapped from.

For example, Fig. 5(a) shows the subset of the original extraneous modes, at their new slowness-frequency coordinates, which fit the theoretical solution, assuming that mode a_0 propagates from the notch to probe 2. The two circled regions show where significant energy matches the theoretical mode matrix—these regions propagate as mode s_0 from laser source to notch, and are converted at the notch to a_0 (and propagate as a_0 from notch to probe 2). Figure 5(b) shows the same modes as Fig. 5(a), but at their original slowness-frequency coordinates. Note that the energy of the incident s_0 mode below 1 MHz is much lower than the incident energy in the a_0 mode in the same frequency range, so this incident s_0 contribution is not obvious in Fig. 2. Figure 6 is a summary of the contributions of all six possible modes, and represents case P2c, with the circles specifying how the original incident Lamb wave is mode converted at the notch.

Now consider the probe 1 measurements that contain the incident and reflected signals. The incident modes (case P1a) are the SFR of probe 1, normalized with propagation dis-

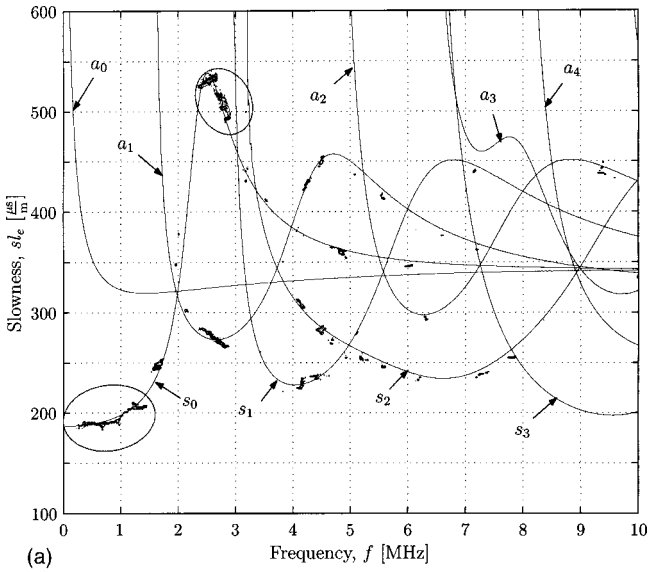

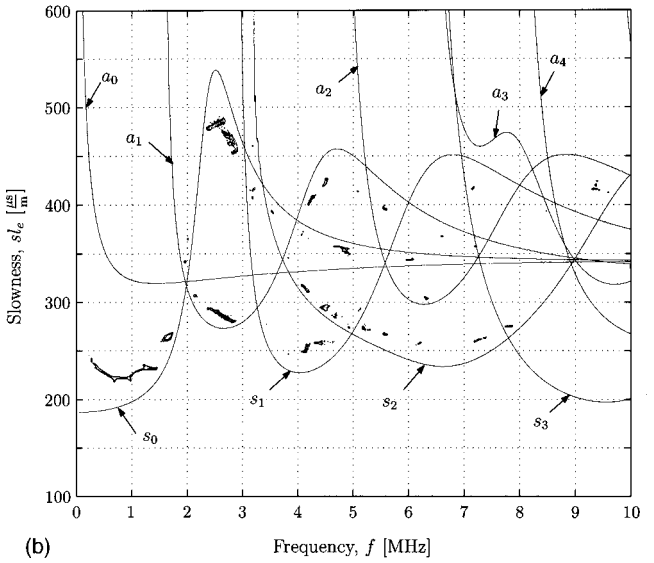

FIG. 5. (a). Subset of extraneous modes (transmitted) assuming mode conversion to mode a_0, new coordinates. (b) The subset of extraneous modes (transmitted) assuming mode conversion to mode a_0, original coordinates.

tance d_1 and shown in Fig. 3(a). The modes in Fig. 3(a) that are close to the theoretical mode lines can be accentuated by multiplying this SFR with the theoretical mode matrix and the resulting SFR is almost identical to Fig. 2, the SFR for the perfect plate.[19] The reflected and non-mode-converted portion (case P1b) of the probe 1 signal is identified by calculating a SFR with the propagation distance d_5, and multiplying with the theoretical mode matrix (to accentuate the modes coinciding with the theoretical solution). These case P1b modes are shown in Fig. 7.

In a procedure similar to case P2c, extraneous modes that cannot be allocated to case P1a (incident modes) or case P1b (reflected, non-mode-converted) are extracted by multiplying the SFR of the reflected signal with the inverse theoretical mode matrix. An automated algorithm similar to the one used for case P2c is developed for case P1c, using a modified version of Eq. (3). The SFR that shows the modes belonging to case P1c, including their converted mode assignment (notch to probe 1) is shown in Fig. 8.

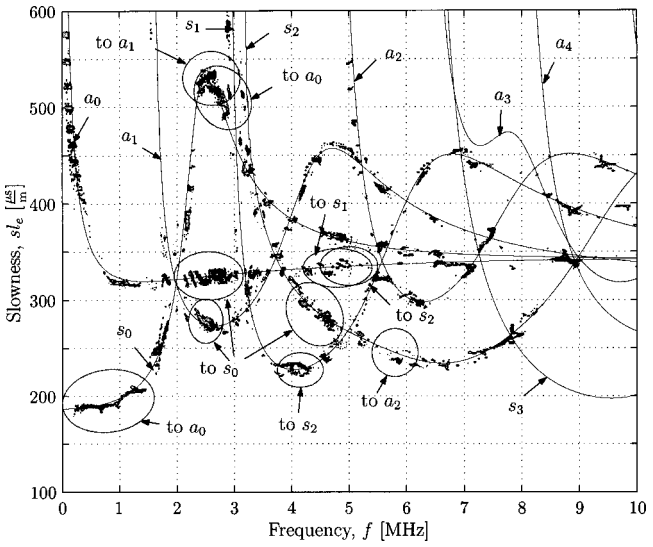

FIG. 6. SFR of modes belonging to case P2c, transmitted and converted.

The non-mode-converted, transmitted, and reflected SFRs (Figs. 4 and 7) are very similar to each other and do not appear to show any definite pattern that can be associated with notch width or depth. There are subtle differences—such as mode a_1 from 2–3 MHz and mode s_1 below 4 MHz are reflected but not transmitted—but it is difficult to make a quantitative interpretation as to how the incident Lamb wave is scattered into reflected and transmitted portions without a predictive theoretical model. However, this comparison is not an objective of this research. More importantly, note that the mode conversion at the notch for both the transmitted and reflected cases are very similar to each other—compare Figs. 6 and 8. This behavior validates the hypothesis that the notch acts as an additional source. Finally, note that a vast majority of the extraneous mode energy is identified with mode conversion,[19] so the amount of incident signal energy that is scattered at the notch as a local frequency shift or as an internal reflection is probably small in comparison.

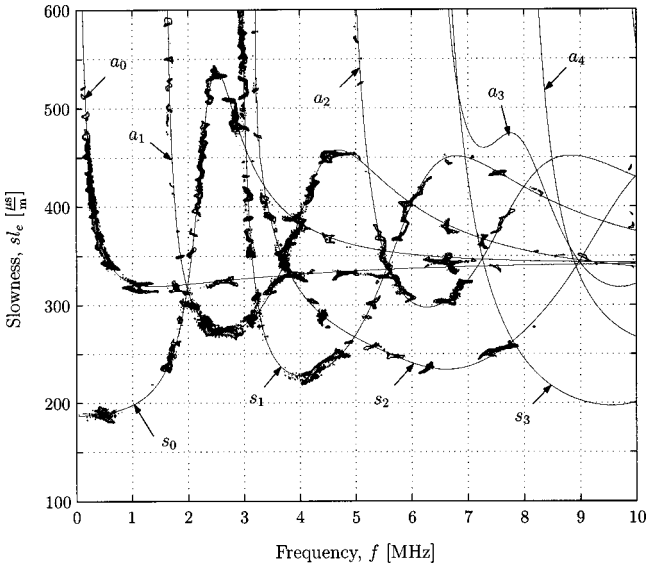

FIG. 7. SFR of modes belonging to case P1b, reflected and non-mode-converted.

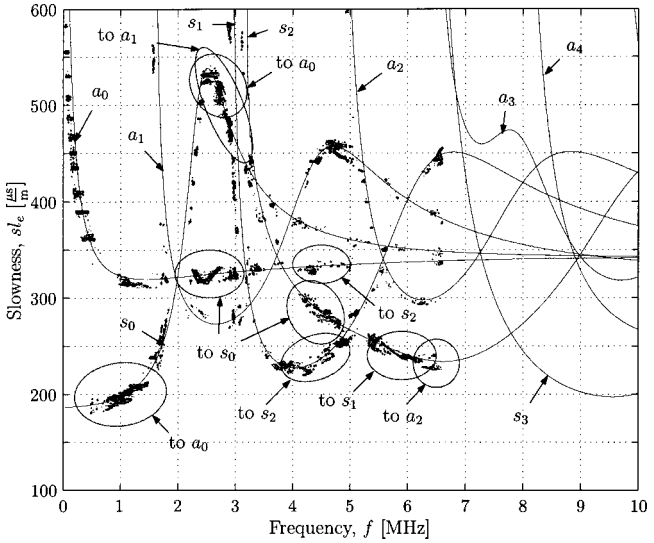

FIG. 8. SFR of modes belonging to case P1c, reflected and converted.

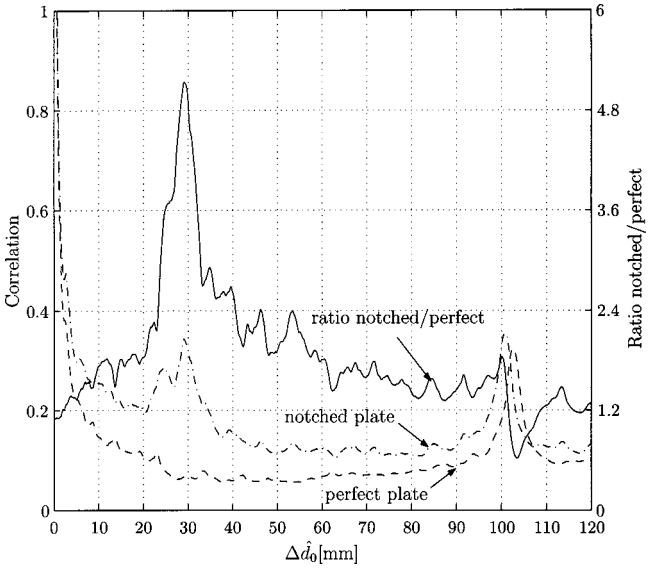

FIG. 9. Correlation curves for the perfect plate, notched plate, and a division of both curves, 0–10 MHz frequency bandwidth, reflected contribution.

IV. LOCALIZATION OF THE NOTCH

An automated localization methodology is now developed based on the understanding of the interaction of a Lamb wave with a notch—note that the notch location is now assumed to be unknown. Previous research[8] formulated a correlation technique that uses the non-mode-converted parts of the reflected modes to locate a notch in a plate. This correlation procedure does not require (nor was it developed with) an understanding of the scattering of a Lamb wave by a notch, and this procedure identifies the position where the non-mode-converted portions (and only these portions) of the reflected modes coincide with the incident modes. The current research uses an understanding of scattering to extend this technique, using, for example, a targeted frequency bandwidth to help refine the localization procedure.

Up until this point, the current research has neglected the width of the notch (the notch is treated as being infinitely thin), and has defined the location of the notch by its centerline (see Fig. 1). The proposed localization technique will be more accurate if the finite width of the notch is taken into account. Introduce three new distances ($\hat{d}_0, \hat{d}_3, \hat{d}_5$) that are based on the near edge (in relation to the laser source) of the notch: $\hat{d}_0 = d_0 - w/2$, $\hat{d}_3 = d_3 - w/2$, and $\hat{d}_5 = d_5 - w$, where w is the notch width. Note that there is no difference in the *visual appearance* of a SFR that is calculated with $\hat{d}_i$ instead of d_i—this small change in propagation distance has no visible effect on the SFRs presented in Figs. 2–8.

First, localize the notch with the reflected wave field by considering the probe 1 signal. Assume that $\Delta\hat{d}_0$ is the unknown distance from probe 1 to the notch. By systematically varying $\Delta\hat{d}_0$ (and the associated propagation distance $d = d_1 + 2\Delta\hat{d}_0$), SFRs are calculated for each distance. Next, correlate each of these SFRs with the incident modes (the SFR calculated with distance d_1), or

$$\mathrm{Corr}(d) = \sum_{sl_e} \sum_{f} \mathrm{SFR}(sl_e, f, d_1) \times \mathrm{SFR}(sl_e, f, d), \quad \forall d. \tag{4}$$

Obviously, this correlation reaches its maximum for a representation calculated with $\Delta\hat{d}_0 = 0$ (the correlation of two identical signals), but reflections (from both the notch and any plate edges) will introduce local maxima in the correlation curve at certain $\Delta\hat{d}_0$'s. These local maxima occur when the reflected modes within the SFR coincide with the incident modes—which, in turn, provides a measure of the receiver to notch distance. At $\Delta\hat{d}_0$ equal to the exact receiver to notch distance $\Delta\hat{d}_0 = \hat{d}_0$, the reflected (but not mode converted, case P1b) contribution matches the incident wave field.

Figure 9 shows the correlation of the SFRs of the notched plate (the dot–dashed line) for $\Delta\hat{d}_0$ varying between 0 and 120 mm with an increment step of 0.2 mm. Each of these SFRs (calculated with a propagation distance $d = d_1 + 2\Delta\hat{d}_0$) are correlated with the same SFR, calculated with $d = d_1$, as defined by Eq. (4). This procedure is repeated for the perfect plate (correlated with the incident modes of the perfect plate) and shown as the dashed line in Fig. 9. The solid line in Fig. 9 represents the ratio of the notched plate correlation curve divided by the perfect plate correlation curve. This ratio curve emphasizes the local maxima caused by features that exist in the notched plate, but not in the perfect plate; maxima in the perfect plate can only be caused by the edges, while maxima in the notched plate can be caused by the notch or the edges. As a result, the maximum of the ratio curve represents the reflection from the notch—the ratio curve has a single dominant peak at $\Delta\hat{d}_0 = 29$ mm (the actual distance is $\hat{d}_0 = 29.2$ mm). This correlation procedure calculates the receiver to notch distance with outstanding accuracy, and the error (0.2 mm) is on the order of the tolerance of the width of the notch.

Further improvement in localization accuracy is achieved using a frequency-limited bandwidth (such as from 0–2 MHz) of the SFRs for the correlations—the results are shown in Fig. 10. Note that the correlations in Fig. 9 use the

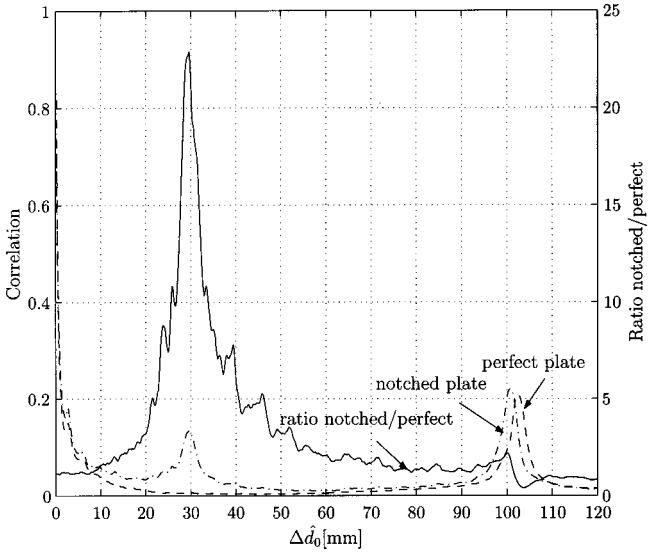

FIG. 10. Correlation curves for the perfect plate, notched plate, and a division of both curves, 0–2 MHz frequency bandwidth, reflected contribution.

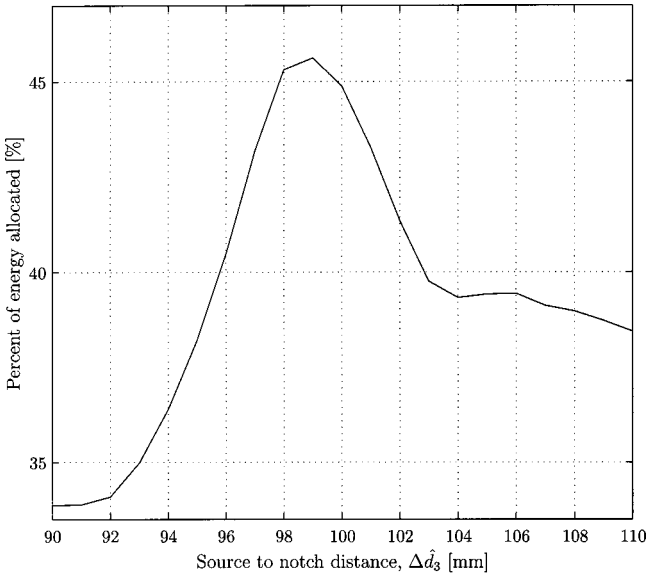

FIG. 11. Goodness-of-fit (as a function of percent allocated) of the allocation of extraneous modes to case P2c, used to locate the notch with a transmitted contribution.

entire frequency bandwidth, 0–10 MHz. This particular (limited-) frequency bandwidth is selected because the case P1b (reflected and non-mode-converted) SFR in Fig. 7 shows significant energy in the frequency bandwidth from 0–2 MHz—the same is also true for the SFR of the incident modes. The peak of the curve representing the ratio of notched/perfect plate in Fig. 10 is still at the same location, but it is now even sharper and its value is almost five times higher than in Fig. 9—the sharpness and value of the maximum are measures of the preciseness of the results. The significance of this frequency bandwidth (0–2 MHz) becomes more evident when correlation curves for the remaining bandwidth (2–10 MHz) are considered, which results in a much wider peak, on the order of 8 mm.[19] Note that the correlation curves in Figs. 9 and 10 are more accurate and definitive than the results presented in Hurlebaus *et al.*[8] These improvements are due to the use of the reassigned spectrogram in this study (as opposed to the unreassigned spectrogram in Hurlebaus *et al.*[8]) as the basis for the SFRs, and the ability to identify a targeted frequency range that contains significant P1b energy.[19]

Now, consider a second localization technique that uses the transmitted wave field of probe 2. Unfortunately, a correlation technique in terms of the case P2b transmitted, non-mode-converted modes is not possible, because the case P2b SFR is calculated with distance d_4, which is independent of notch location. Instead, consider a technique based on the goodness-of-fit when allocating the extraneous modes to case P2c, transmitted and mode converted. Assume that $\Delta\hat{d}_3$ is the unknown source to notch distance; varying $\Delta\hat{d}_3$ can be used to define a measure (as a function of distance) of how well portions of the extraneous modes can be allocated to case P2c. For each $\Delta\hat{d}_3$, a modified version of the allocation algorithm for case P2c [that uses Eq. (3) and is described in the previous section] is performed on the transmitted signal. Specifically, the goodness-of-fit for any $\Delta\hat{d}_3$ is given by summing the maximum possible magnitudes of the theoretical mode matrix, $T(sl_e, f)$, for the mapping of all the slowness-frequency pairs specified by the extraneous P2c modes being classified. Dividing this value by the number of slowness-frequency pairs to be mapped is the goodness-of-fit measure. A value of 100% means perfect mapping, with all the extraneous modes mapped perfectly to the theoretical solution. In reality, lower percentages will be obtained because of experimental uncertainties and the possibility that an extraneous mode is mapped to, but not exactly on top of the theoretical Rayleigh–Lamb solution.

Figure 11 shows the curve representing the percentage of energy that is allocated to the extraneous modes, as a function of source to notch distance, $\Delta\hat{d}_3$—there is a clear peak near the correct distance, $\Delta\hat{d}_3 = d_3 = 99.2$ mm. Note that this technique does not require an experimental signal from the perfect plate, but it does need the theoretical solution of Lamb modes in a perfect plate. Additionally, the success of this technique validates the accuracy of the assignment of the extraneous modes into case P2c in Sec. III.

V. CONCLUSION

This research establishes the effectiveness of combining laser ultrasonic techniques with a SFR to locate a notch in a plate. The high fidelity, broad-bandwidth, point-like, and noncontact nature of laser ultrasonics are critical to the success of this study. The dual-probe laser interferometer allows for the simultaneous interrogation of both the reflected and transmitted wave fields. The distance invariance of a SFR enables a quantitative interpretation of the scattering of a broadband, incident Lamb wave by a notch. The systematic (and unbiased) mode allocation procedure developed in this research establishes which modes are transmitted and reflected by the notch (and through which frequencies), and identifies which modes are mode converted.

Two automated localization methodologies are developed using this understanding of the scattering of Lamb waves. One technique isolates the contributions of the signal

reflected from the notch by performing a correlation of a series of SFR spectra, each calculated with different, assumed propagation distances. This correlation technique is refined with an understanding of which modes are reflected, but not mode converted (and through which frequencies). A second localization technique uses a goodness-of-fit metric when determining how the transmitted extraneous modes are mode converted. A combination of these two localization techniques is very robust, because it can use either the reflected or transmitted wave fields, or both—this allows for two independent measures of notch location, and can interrogate a variety of source, receiver, and notch, geometric relationships.

ACKNOWLEDGMENT

The Deutscher Akademischer Austausch Dienst (DAAD) provided partial support to Rüdiger Benz.

[1] D. E. Chimenti, ''Guided waves in plates and their use in materials characterization,'' Appl. Mech. Rev. **50**, 247–284 (1997).
[2] L. Cohen, *Time–Frequency Analysis* (Prentice–Hall, Englewood Cliffs, NJ, 1995).
[3] M. Niethammer, L. J. Jacobs, J. Qu, and J. Jarzynski, ''Time–frequency representations of Lamb waves,'' J. Acoust. Soc. Am. **109**, 1841–1847 (2001).
[4] W. H. Prosser, M. D. Seale, and B. T. Smith, ''Time–frequency analysis of the dispersion of Lamb modes,'' J. Acoust. Soc. Am. **105**, 2669–2676 (1999).
[5] M. Lemistre and D. Balageas, ''Structural health monitoring based on diffracted Lamb waves analysis by discrete wavelet transform,'' in *System Identification and Structural Health Monitoring*, edited by A. Guemes (Graficas, Madrid, 2000), pp. 561–569.
[6] P. D. Wilcox, R. P. Dalton, M. J. S. Lowe, and P. Cawley, ''Mode selection and transduction for structural monitoring using Lamb waves'' in *Structural Health Monitoring 2000*, edited by F.-K. Chang (Technomics, New York, 1999), pp. 703–712.
[7] C. Valle, M. Niethammer, J. Qu, and L. J. Jacobs, ''Crack characterization using guided circumferential waves,'' J. Acoust. Soc. Am. **110**, 1282–1290 (2001).
[8] S. Hurlebaus, M. Niethammer, L. J. Jacobs, and C. Valle, ''Automated methodology to locate notches with Lamb waves,'' Acoust. Res. Lett. Online **2**, 97–102 (2001).
[9] S. W. Liu, S. K. Datta, and T. H. Ju, ''Transient scattering of Rayleigh–Lamb waves by a surface-breaking crack: comparison of numerical simulation and experiment,'' J. Nondestruct. Eval. **10**, 111–126 (1991).
[10] Y. Cho and J. L. Rose, ''An elastodynamic hybrid boundary element study for guided wave interactions with a surface breaking defect,'' Int. J. Solids Struct. **37**, 4103–4124 (2000).
[11] M. J. S. Lowe and O. Diligent, ''Low-frequency reflection characteristics of the s_0 Lamb wave from a rectangular notch in a plate,'' J. Acoust. Soc. Am. **111**, 64–74 (2002).
[12] O. Diligent, T. Grahn, A. Boström, P. Cawley, and M. J. S. Lowe, ''The low-frequency reflection and scattering of the S_0 Lamb mode from a circular through-thickness hole in a plate: Finite element, analytical and experimental studies,'' J. Acoust. Soc. Am. **112**, 2589–2601 (2002).
[13] M. Castaings, E. Le Clezio, and B. Hosten, ''Modal decomposition method for modeling the interaction of Lamb waves with cracks,'' J. Acoust. Soc. Am. **112**, 2567–2582 (2002).
[14] D. Alleyne and P. Cawley, ''A two-dimensional Fourier transform method for measurement of propagating multimode signals,'' J. Acoust. Soc. Am. **89**, 1159–1168 (1991).
[15] C. Eisenhardt, L. J. Jacobs, and J. Qu, ''Application of laser ultrasonics to develop dispersion curves for elastic plates,'' J. Appl. Mech. **66**, 1043–1045 (1999).
[16] C. B. Scruby and L. E. Drain, *Laser Ultrasonics: Techniques and Applications* (Adam Hilger, Bristol, 1990).
[17] D. A. Bruttomesso, L. J. Jacobs, and R. D. Costley, ''Development of an interferometer for acoustic emission testing,'' J. Eng. Mech. **119**, 2303–2316 (1993).
[18] S. Hurlebaus, ''A contribution to structural health monitoring using elastic waves,'' Doctoral thesis, University of Stuttgart, Stuttgart, Germany, 2002.
[19] R. Benz, ''Localization of notches with Lamb waves,'' Masters thesis, Georgia Institute of Technology, Atlanta, Georgia, 2002.
[20] F. Auger and P. Flandrin, ''Improving the readability of time–frequency and time-scale representations by the reassignment method,'' IEEE Trans. Signal Process. **43**, 1068–1089 (1995).
[21] R. D. Mindlin, ''Waves and vibrations in isotropic elastic plates,'' in *Structural Mechanics*, edited by J. N. Goodier and N. J. Hoff (Pergamon, New York, 1960).